

# A Parameterised Quantum Circuit Approach to Point Set Matching

Mohammadreza Noormandipour <sup>\*1</sup> Hanchen Wang <sup>\*2</sup>

## Abstract

Point set registration is one of the challenging tasks in areas such as pattern recognition, computer vision and image processing. Efficient performance of this task has been a hot topic of research due to its widespread applications. We propose a parameterised quantum circuit learning approach to point set matching problem. The proposed method benefits from a kernel-based quantum generative model that: 1) is able to find all possible optimal matching solution angles, 2) is potentially able to show quantum learning supremacy, and 3) benefits from kernel-embedding techniques and integral probability metrics for the definition of a powerful loss function. Moreover, the theoretical framework has been backed up by satisfactory preliminary and proof of concept experimental results.

## 1. Introduction

With appearance of Noisy Intermediate Scale Quantum (NISQ) (Preskill, 2018) technologies with tens of working (but noisy) qubits, research has been conducted around possible applications of NISQ devices that can demonstrate a quantum computational advantage (i.e., quantum supremacy) over the classical computers. NISQ devices can be used for gate-based quantum computation algorithms and if a quantum algorithm gives a relatively efficient solution to a problem that is not tractable with classical computers in polynomial time, a quantum advantage is achieved.

The field of quantum machine learning (QML) (Wittek, 2014; Biamonte et al., 2017) explores how to devise and implement machine learning algorithms on quantum systems (Arute et al., 2019; Zhong et al., 2020; Noormandipour, 2020) that could enable a quantum supremacy. This should not be confused with the research on using classical ma-

chine learning algorithms to understand the properties of the quantum systems (Torlai et al., 2018; Noormandipour et al., 2021), however, the effort in this paper is to use quantum computing algorithms to solve a classical problem on classical datasets.

It is argued that the mathematical structure of QML algorithms is fundamentally very similar to that of classical kernel methods (Schuld, 2021). Kernel methods have been widely used in for purposes such as dimensional reduction in classical machine learning (Hofmann et al., 2008) as well as neural networks (Cho & Saul, 2009; Belkin et al., 2018). Samples from a classical dataset can be mapped to a *reproducing kernel Hilbert space (RKHS)* with a suitable *feature map*, where they can be compared more efficiently and a kernel is simply defined as the inner product of two points in the RKHS. By defining a quantum feature map, we can obtain a quantum RKHS and hence, a quantum kernel. Kernel-based quantum models are supposed to have a more efficient training than the variational quantum circuit models (Schuld, 2021) and therefore need less training parameters. This is of importance in hybrid-quantum classical models (models with a classical optimisation routine) on NISQ devices, since due to existence of decoherence in these devices, the circuits should be kept as shallow as possible.

In this paper, we use a parameterised quantum circuit (PQC) model with a classical and quantum kernel-based loss function to solve a point set matching problem. A precise definition of the problem statement is given in section 2. The solution of the problem is mapped to the output quantum distribution of the PQC and the training is performed via quantum gradient-based minimization of the loss function. In order to compare the empirical and rotated point sets, the coordinates of the points in the point clouds have been mapped to a (Quantum) RKHS, via a (quantum) feature map and then a kernel correlation approach is incorporated to define a distance function between the point sets. This distance function is then used in an *Integral Probability Metric (IPM)* to define the final loss function. The gradient of the loss function is evaluated via a quantum circuit with a similar structure as the main PQC used for obtaining the output solution distribution to the problem.

The perfect point set correspondence problem is an NP-hard

<sup>\*</sup>Equal contribution <sup>1</sup>TCM Group, Cavendish Laboratory, University of Cambridge, J.J. Thomson Avenue, Cambridge CB3 0HE, United Kingdom <sup>2</sup>Department of Engineering, University of Cambridge, Cambridge, UK.. Correspondence to: Mohammadreza Noormandipour <mrn31@cam.ac.uk>.

problem. The proposed approach to find the solution for this problem has been tested on 2D and 3D symmetric and asymmetric shaped point sets and it has been shown that it can pinpoint the *multiple* correct solutions for the problem, which has been done for the first time. Moreover, this is the first QML approach to the problem and it is potentially capable of showing quantum computational advantage upon efficient implementation on quantum hardware.

In what follows, we first try to give a concrete statement for the problem and set the initial notations in section 2, then we will explain in detail a kernel correlation based approach in section 3, which is an effective classical method. Then the parameterised quantum circuit approach to the problem and implementation of it is discussed in section 4. This quantum approach is guaranteed to efficiently find the global minimum of the particular loss that we will define for it. Finally, the experiments and results are presented in section 5 along with a short discussion in section 6.

## 2. Problem Statement

Point set registration is one of the key tasks in computer vision, pattern recognition, robotics and image processing (Zhu et al., 2019). In this section, we formulate the task of point set registration, highlighting how previous methods solve its most challenging part, which is to find out the point pair correspondence between the two sets.

We use  $\mathcal{M}$  and  $\mathcal{S}$  to denote two point sets, where  $\mathcal{M} = \{\mathbf{m}_i\}_{i=1}^N \subset \mathbb{R}^2$  or  $\mathbb{R}^3$  and  $\mathcal{S} = \{\mathbf{s}_i\}_{i=1}^{N'} \subset \mathbb{R}^2$  or  $\mathbb{R}^3$ . For the ease of notations, we consider the simplest case, in which  $N = N'$ , we later discuss the extension when  $N \neq N'$ .

Assuming  $\mathcal{M}$  is transformed from  $\mathcal{S}$  via an unknown rigid transformation:  $\mathcal{T} = [\mathbf{r}_{\mathcal{MS}}, \mathbf{t}_{\mathcal{MS}}]$ , where  $\mathbf{r}_{\mathcal{MS}} \in \text{SO}(2)$  or  $\text{SO}(3)$  and  $\mathbf{t}_{\mathcal{MS}} \in \mathbb{R}^2$  or  $\mathbb{R}^3$ . The objective of this task is to minimise the matching error  $\mathcal{L}$ , e.g., mean-squared, between  $\mathcal{M}$  and  $\mathcal{S}$  under some correspondence.

A point pair correspondence function  $L_{\mathcal{MS}}$  is used to find the corresponding point(s) in  $\mathcal{S}$  for each point  $\mathbf{m}_i$  in  $\mathcal{M}$ :

$$L_{\mathcal{MS}} : \mathcal{M} \rightarrow \mathcal{S} \quad (1)$$

for the simplicity we assume  $L_{\mathcal{MS}}$  is bijective ( $N = N'$ ):  $L_{\mathcal{MS}}(\mathbf{m}_i) = \mathbf{s}_j$ , which is the setting in most prior works. A more comprehensive configuration is to return multiple corresponding points in  $\mathcal{S}$  for each query point  $\mathbf{m}_i$  in  $\mathcal{M}$ :

$$L_{\mathcal{MS}}(\mathbf{m}_i) = \{\mathbf{s}_{j_k}\}_{k=1}^K \quad (2)$$

This is also known as multi-linked/scaled (Granger & Penne, 2002) or SoftAssignment (Rangarajan et al., 1997). It is more robust when encountered with real world data collected from scanners, where the exact point pair correspondence does not exist, therefore it is also used in recent works (Tsin & Kanade, 2004; Golyanik & Theobalt, 2020).

With  $L_{\mathcal{MS}}$  defined, we can directly solve the optimal  $\mathcal{T}^{opt}$  that results in the lowest matching error between  $\mathcal{M}$  and  $\mathcal{S}$ :

$$\left( \frac{\partial}{\partial \mathcal{T}} \sum_{\mathbf{m}_i \in \mathcal{M}} \|\mathcal{T}\mathbf{m}_i - L_{\mathcal{MS}}(\mathbf{m}_i)\|_2 \right) \Big|_{\mathcal{T}=\mathcal{T}^{opt}} = 0 \quad (3)$$

where  $\mathcal{T}\mathbf{m}_i := \mathbf{r}_{\mathcal{MS}} \cdot \mathbf{m}_i + \mathbf{t}_{\mathcal{MS}}$ . The ground truth of the transformation  $\mathcal{T}^{gt}$  is also calculated in this fashion based on the provided rather than the predictive correspondence<sup>1</sup>. Clearly if the predictive correspondence is the same as the ground truth, it is deterministic as well as model-agnostic to solve  $\mathcal{T}^{opt}$  which achieves the lowest matching error. However, finding such correspondence mapping for a perfect matching is known as a NP-hard problem.

## 3. Classical Kernel Correlation Approach

Correlation-based measures has been widely used for image (Brown, 1992) and point set (Tsin & Kanade, 2004) registration. We begin with introducing the classical kernel based method (Tsin & Kanade, 2004) and then in following sections we describe how one can improve this method and define a quantum kernel.

(Tsin & Kanade, 2004) extend the correlation technique to point set registration with Kernel Correlation (KC), which is a measure of affinity as well as a function of the point set entropy. KC between two points,  $\mathbf{x}_i$  and  $\mathbf{x}_j$ , is defined as:

$$\mathcal{KC}(\mathbf{x}_i, \mathbf{x}_j) = \int_{\mathbb{R}^2 \text{ or } \mathbb{R}^3} K(\mathbf{x}, \mathbf{x}_i) K(\mathbf{x}, \mathbf{x}_j) d\mathbf{x} \quad (4)$$

where  $K(\cdot, \cdot)$  is a kernel function such as Gaussian, RBF and Laplacian. We use Gaussian kernels as an example:

$$\mathcal{KC}_G(\mathbf{x}, \mathbf{x}_i) = (\pi\sigma^2)^{-D/2} \exp(-\|\mathbf{x} - \mathbf{x}_i\|_2^2/\sigma^2) \quad (5)$$

the homologic kernel correlation then can be written as:

$$\mathcal{KC}_G(\mathbf{x}_i, \mathcal{X}) = (\pi\sigma^2)^{-D/2} \exp(-\|\mathbf{x}_i - \mathbf{x}_j\|_2^2/\sigma^2) \quad (6)$$

Next we introduce the KC between a point and the whole point set  $\mathcal{X}$ , the Leave-one-out Kernel Correlation (L-KC):

$$\mathcal{KC}(\mathbf{x}_i, \mathcal{X}) = \sum_{\mathbf{x}_j \neq \mathbf{x}_i} \mathcal{KC}(\mathbf{x}_i, \mathbf{x}_j) \quad (7)$$

Leave-one-out KC defines the *total affinity* from a point to a point set. The KC of a point set is defined as the total sum of the L-KC of all the points  $x_k$  in the set:

$$\mathcal{KC}(\mathcal{X}) = \sum_i \mathcal{KC}(\mathbf{x}_i, \mathcal{X}) = 2 \sum_{i \neq j} \mathcal{KC}(\mathbf{x}_i, \mathbf{x}_j) \quad (8)$$

<sup>1</sup>point/fragment correspondence is usually provided for testing, e.g., 3DMatch (Zeng et al., 2017) and KITTI (Geiger et al., 2012)

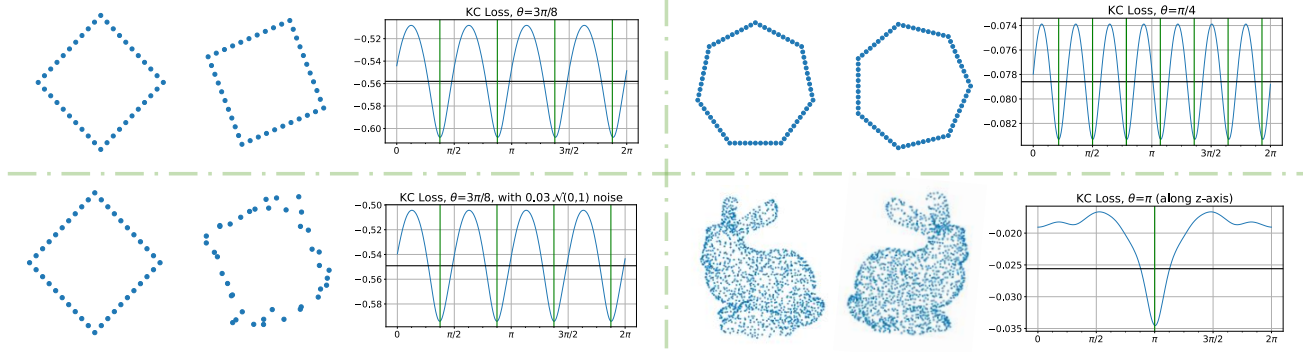


Figure 1. Illustration on kernel correlation loss: Left column shows that KC loss is successful in finding the 4 correct matching angles for a rotated square even in the presence of noise (bottom-left panel). The right column shows the effectiveness of KC loss for more complicated shapes, namely a heptagon and a 3D bunny shape.

If the points in the set are close to each other, the KC value is large. In this sense KC of a point set is a compactness measure of the point set.

The best transformation  $\mathcal{T}^{opt}$  for aligning  $\mathcal{M}$  and  $\mathcal{S}$  is solved via searching for the minimum of the following loss:

$$\mathcal{T}^{opt} = \arg \min \left( - \sum_{s \in \mathcal{S}} \sum_{m \in \mathcal{M}} \mathcal{KC}(\mathcal{T}m, s) \right) \quad (9)$$

Notice that in the above equation each transformed model point  $m$  is interacting with all the scene points. We call (9) a multiply-linked registration cost function. This is in contrast to the ICP styles (Besl & McKay, 1992; Chen & Medioni, 1991; Zhang, 1994), where each model point is connected to its nearest scene point only.

By denoting the kernel density estimates (KDE) as:

$$P_{\mathcal{M}}(x, \theta) = \sum_{m \in \mathcal{M}} K(x, T(m, \theta)) / N \quad (10)$$

$$P_{\mathcal{S}}(x) = \sum_{s \in \mathcal{S}} K(x, s) / N \quad (11)$$

We observe that:

$$\begin{aligned} & N^2 \int_x (P_{\mathcal{M}} - P_{\mathcal{S}})^2 dx \\ &= N^2 \left( \int_x P_{\mathcal{M}}^2 dx + \int_x P_{\mathcal{S}}^2 dx - 2 \int_x P_{\mathcal{M}} \cdot P_{\mathcal{S}} dx \right) \quad (12) \\ &= 2 \cdot \mathcal{L}(\mathcal{T}\mathcal{M}, \mathcal{S}) + \text{Constant} \end{aligned}$$

where  $\mathcal{L}$  is the loss defined in (9). Notice that the first two terms in the second line of (12) evaluate to constants as they are related to individual rigid point sets. Minimising the left side of (15) is equivalent to minimising our registration cost function.

## 4. Quantum Circuit Learning Approach

In this section, we use the concepts of learning and modelling in the language of Quantum Circuit Learning (QCL) (Mitarai et al., 2018; Farhi & Neven, 2018) and we use a *Parameterised Quantum Circuit (PQC)* model (Coyle et al., 2020) and its variants to find the solution to a point set matching problem. Furthermore, the details of using the classical kernel correlation as well as a quantum kernel to define an efficient loss function through integral probability metrics are also discussed and the procedure for calculation of the gradient of the loss function for training is presented in details. The curious reader can have a look at the arXiv version of (Coyle et al., 2020) or some background knowledge, such as the classical simulation of the quantum computations happening in the QCL and the discussion around supremacy of quantum learning and how it provides an advantage over the conventional approaches.

In appendix A, we also have briefly explained a separate quantum-based attempt to solve the point set matching problem, by formulating it in the form of an objective function for a *quadratic unconstrained binary optimisation problem (QUBOP)* and minimizing this objective on an *Adiabatic Quantum Annealer (AQA)* (Golyanik & Theobalt, 2020).

### 4.1. Quantum Circuit Born machine

After solving the translation transformation between two point sets by matching their centre of mass, one needs to find the optimal rotation angles to match these two sets. In order to be able to use the NISQ devices for this purpose, we will encode the solution of our problem into the output distribution of a PQC. This class of circuits have variational parameters that can be optimised with a classical optimisation routine to get the desired output distribution. In other words, we are proposing a quantum machine learning algorithm to solve the point set matching problem that has a quantum supremacy over the classical approaches to this

problem.

We adapt a subclass of PQCs which is a generative quantum-classical hybrid learning model called *Quantum Circuit Born Machine (QCBM)* (Cheng et al., 2018; Liu & Wang, 2018a). As shown in Fig. 2, a generic QCBM consists of an  $n$ -qubit state initialised in  $|0\rangle$  state,  $|\psi_{in}\rangle = |0\rangle^{\otimes n}$  and layers of parameterised unitary gates.

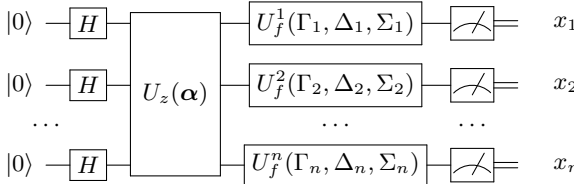


Figure 2. A generic layout of a parameterised quantum circuit.

The first layer is a series of Hadamard gates to produce equal amplitude superpositions of computational basis vectors and the  $U_z(\cdot)$  and  $U_f(\cdot, \cdot, \cdot)$  gates are defined in (13), (14).

$$U_z(\alpha) := \prod_j U_z(\alpha_j, S_j) = \prod_j \exp \left( i\alpha_j \bigotimes_{k \in S_j} Z_k \right) \quad (13)$$

$$U_f(\Gamma, \Delta, \Sigma) := \exp \left( i \sum_{k=1}^n \Gamma_k X_k + \Delta_k Y_k + \Sigma_k Z_k \right) \quad (14)$$

where  $X_k, Y_k, Z_k$  are the Pauli operators acting on the  $k$ -th qubit and  $S_j$  is a subset of the qubits in the quantum register.

Measuring the output state of the above circuit in computational basis gives a binary vector  $\mathbf{x}$  and for  $n$  qubits in the quantum register, there are a total of  $2^n$  number of possible vectors. We split the range  $[0, 2\pi)$  of rotation angle around the  $\hat{z}$  axis to  $2^n$  number of bins and then we identify the binary vectors with these bin values. For example, if the measurement outcome of a 4 qubit circuit is  $\mathbf{x} = (0, 1, 0, 1)$ , the corresponding rotation angle becomes  $\theta = \frac{(1 \times 2^0 + 1 \times 2^2)}{2^4} \times 2\pi$ . The resolution for the rotation angle is  $\Delta\theta = \frac{2\pi}{2^n}$ , which exponentially improves with increasing the number of qubits in the quantum register.

Based on the Born rule from quantum mechanics, the distribution of the binary vectors,  $p_\eta(\mathbf{x})$ , which is parameterised by the set of angles  $\eta = \{\alpha, \Gamma, \Delta, \Sigma\}$  is explicitly given by

$$p_\eta(\mathbf{x}) := \left| \langle \mathbf{x} | U_f(\Gamma, \Delta, \Sigma) U_z(\alpha) H^{\otimes n} | 0 \rangle^{\otimes n} \right|^2 \quad (15)$$

For universal quantum computation we just need to restrict to single- and two-qubit gates (meaning that  $|S_j| \leq 2$ ), and the argument of the  $U_z(\cdot)$  gate reduces to the Ising Hamiltonian and the circuit is called Quantum Circuit Ising Born Machine (QCIBM) (Coyle et al., 2020).

$$\mathcal{H} = i \sum_{i < j} J_{ij} Z_i Z_j + i \sum_{k=1}^n b_k Z_k \quad (16)$$

By particular choice of parameters  $\eta$ , a QCIBM can reduce to other circuit sub-classes such as instantaneous quantum polynomial time (IQP) (Shepherd & Bremner, 2009) circuits and quantum approximate optimisation algorithm (QAOA) (Farhi et al., 2014) circuits. Both of these sub-classes are expected to demonstrate quantum supremacy (Bremner et al., 2017; Farhi & Harrow, 2016). More on this will come in the experiments section.

## 4.2. Kernel embedding and defining the loss function

As previously mentioned, the point set registration is being performed through learning the distribution of possible rotation angles that matches the scene and the model sets. For a given rotation angle, in order to calculate the closeness of two point sets, we need to encode the coordinates of the points in the point sets to states in the Hilbert space and then compare them. Hence, here we aim to explain the details of kernel embedding procedure (Muandet et al., 2017) and we use a similar definition of a quantum feature map from data sample space to Hilbert space which was first introduced in (Schuld & Killoran, 2019). This will allow us to define a quantum kernel.

**Definition 4.1** (*Quantum Feature Map and the Quantum Kernel*). *Let  $\Phi : \mathcal{X} \rightarrow \mathcal{H}_Q$  be a quantum feature map over an input set  $\mathcal{X}$ , giving rise to a real-valued quantum kernel product:  $\kappa_Q(\mathbf{x}, \mathbf{y}) := |\langle \Phi(\mathbf{x}) | \Phi(\mathbf{y}) \rangle|^2$ .*

The existence of the quantum feature map and hence a quantum kernel in a unique Quantum RKHS is guaranteed by the Theorems 1 and 2 in (Schuld & Killoran, 2019).

In order to increase the chance of observing quantum advantage, we use a kernel, firstly introduced in (Havlíček et al., 2019), which is classically difficult to calculate. The feature map for this kernel can be computed with the following quantum circuit:

$$\Phi : \mathbf{x} \in \mathcal{X} \rightarrow |\Phi(\mathbf{x})\rangle \in \mathcal{H} \quad (17)$$

$$|\Phi(\mathbf{x})\rangle := U_{\Phi(\mathbf{x})} H^{\otimes n} U_{\Phi(\mathbf{x})}^* |0\rangle^{\otimes n} \quad (18)$$

where the unitary encoding operators  $U_{\Phi(\mathbf{x})}$  are chosen in such a way that the circuit required to calculate them is structurally similar to the Ising Born Machine (IBM). The

similar choice of circuits is experimentally favourable, because we are avoiding the preparation cost for two different circuits at hardware level.

$$U_{\Phi(\mathbf{x})} := \exp \left( i \sum_{S \subseteq [n]} \phi_S(\mathbf{x}) \prod_{i \in S} Z_i \right) \quad (19)$$

The explicit form of the single- and two-qubit gates,  $U_{\phi_{\{k\}}(\mathbf{x})}$  and  $U_{\phi_{\{l,m\}}(\mathbf{x})}$  is

$$\begin{aligned} U_{\phi_{\{k\}}(\mathbf{x})} &= \exp(i\phi_{\{k\}}(\mathbf{x})Z_k) \\ U_{\phi_{\{l,m\}}(\mathbf{x})} &= \exp(i\phi_{\{l,m\}}(\mathbf{x})Z_l \otimes Z_m) \end{aligned} \quad (20)$$

where the encoding of the classical samples is performed via

$$\phi_{\{k\}}(\mathbf{x}) := \frac{\pi}{4}x_k, \quad \phi_{\{l,m\}}(\mathbf{x}) := \left(\frac{\pi}{4} - x_l\right)\left(\frac{\pi}{4} - x_m\right) \quad (21)$$

Next, we need to define an efficient cost function to train the QIBM. One of the well-known discrepancy functions between two distributions is the KL divergence, but as shown in (Liu & Wang, 2018b; Mitra et al., 2018), sampling the probabilities require to calculate the gradient of  $\mathcal{L}_{\text{KL}}$  is  $\# \mathbf{P}$ -hard and therefore, to solve this issue an alternative class of discrepancy functions called *Integral Probability Metrics* (IPM) is used in (Coyle et al., 2020). The general form of IPMs between two distributions  $P$  and  $Q$  can be written as:

$$\gamma_{\mathcal{F}}(P, Q) = \sup_{\phi \in \mathcal{F}} (\mathbb{E}_P[\phi] - \mathbb{E}_Q[\phi]) \quad (22)$$

where the class of functions  $\mathcal{F}$ , defines the metric. For example, for some frequently used metrics, such as *Maximum Mean Discrepancy* (MMD), *Total Variation* (TV), and *Kantorovich*, we have:

$$\begin{aligned} \mathcal{F}_{\text{MMD}} &= \{\phi \in \mathcal{H} : \|\phi\|_{\mathcal{H}} \leq 1\} \\ \mathcal{F}_{\text{TV}} &= \{\phi : \|\phi\|_{\infty} \leq 1\} \\ \mathcal{F}_{\text{K}} &= \{\phi : \|\phi\|_L \leq 1\} \end{aligned} \quad (23)$$

By restricting the feature map used to calculate the quantum kernel in definition 4.1, to embed the samples to a unit sphere in Hilbert space (and hence getting the  $\mathcal{F}_{\text{MMD}}$ ), it can be shown that the metric for MMD is the difference in mean embedding between the two distributions (Gretton et al., 2012; Borgwardt et al., 2006):

$$\gamma_{\text{MMD}}(P, Q) = \|\mu_P - \mu_Q\|_{\mathcal{H}} \quad (24)$$

Then we can define a cost function for MMD as:

$$\begin{aligned} \mathcal{L}_{\text{MMD}} &:= \gamma_{\text{MMD}}(P, Q)^2 = \|\mathbb{E}_P[\phi(\mathbf{x})] - \mathbb{E}_Q[\phi(\mathbf{x})]\|_{\mathcal{H}}^2 \\ &= \mathbb{E}_{\substack{\mathbf{x} \sim P \\ \mathbf{y} \sim Q}} (\kappa(\mathbf{x}, \mathbf{y})) + \mathbb{E}_{\substack{\mathbf{x} \sim Q \\ \mathbf{y} \sim P}} (\kappa(\mathbf{x}, \mathbf{y})) - 2\mathbb{E}_{\substack{\mathbf{x} \sim P \\ \mathbf{y} \sim Q}} (\kappa(\mathbf{x}, \mathbf{y})) \end{aligned} \quad (25)$$

where  $\kappa(\cdot, \cdot)$  is the kernel associated with MMD. The kernel used to calculate the MMD loss,  $\mathcal{L}_{\text{MMD}}$ , should be *bounded*, *measurable* and *characteristic* (Sriperumbudur et al., 2009). For the case of quantum kernel, this has been ensured with the particular choice of the quantum feature map defined in (18). Moreover, for the classical kernel correlation (4), these conditions are satisfied by using a Gaussian kernel (which is characteristic (Sriperumbudur et al., 2009)) in (4) and also re-scaling the coordinates of the points in point sets, as illustrated in figure 1.

In the next subsection, we would like to combine the results of section 3 for the classical kernel correlation with (25) and derive an explicit form for the gradients of  $\mathcal{L}_{\text{MMD}}$ . One can write the same derivation for the quantum kernel  $\kappa_Q$ . We re-write the  $\mathcal{L}_{\text{MMD}}$  as:

$$\mathcal{L}_{\text{MMD}} = \mathbb{E}_{\substack{\mathbf{x} \sim P \\ \mathbf{y} \sim P}} (\mathcal{K}\mathcal{C}(\mathbf{x}, \mathbf{y})) + \mathbb{E}_{\substack{\mathbf{x} \sim Q \\ \mathbf{y} \sim Q}} (\mathcal{K}\mathcal{C}(\mathbf{x}, \mathbf{y})) - 2\mathbb{E}_{\substack{\mathbf{x} \sim P \\ \mathbf{y} \sim Q}} (\mathcal{K}\mathcal{C}(\mathbf{x}, \mathbf{y})) \quad (26)$$

where  $P$  and  $Q$  are practically the original point set  $\mathcal{S}$  (Scene) and its transformed version  $\mathcal{M}$  (Model) as described in section 2.

### 4.3. Training Procedure

With a loss function based on MMD metric, we need to evaluate its gradient w.r.t the parameters of the QCL model to perform optimisation via gradient descent. Similar to (Sriperumbudur et al., 2009), given the point sets  $\mathcal{M} = \{\mathbf{x}^1, \dots, \mathbf{x}^N\}$  and  $\mathcal{S} = \{\mathbf{y}^1, \dots, \mathbf{y}^M\}$ , we can estimate the empirical cost  $\tilde{\mathcal{L}}_{\text{MMD}}$ :

$$\begin{aligned} \tilde{\mathcal{L}}_{\text{MMD}} &= \tilde{\gamma}_{\text{MMD}}(\mathcal{M}, \mathcal{S})^2 = \frac{1}{N(N-1)} \sum_{i \neq j}^N \mathcal{K}\mathcal{C}(\mathbf{x}^i, \mathbf{x}^j) \\ &\quad + \frac{1}{M(M-1)} \sum_{i \neq j}^M \mathcal{K}\mathcal{C}(\mathbf{y}^i, \mathbf{y}^j) - \frac{2}{MN} \sum_i^N \sum_j^M \mathcal{K}\mathcal{C}(\mathbf{x}^i, \mathbf{y}^j) \end{aligned} \quad (27)$$

where  $\mathcal{K}\mathcal{C}(\cdot, \cdot)$  is defined in (4). Similar to (12), the first two terms in (27) are constants since the exponent of the Gaussian used in  $\mathcal{K}\mathcal{C}$  always evaluates to zero, hence we discard these two terms from the loss.

The result of the measurement of the Born circuit output state  $|\psi_{\text{out}}\rangle$  is mapped to the valid range for the  $\theta$  (i.e.,  $[0, 2\pi)$ ), the parameter for rotations around the  $\hat{z}$  axis, for 2D and 3D point sets. We obtain  $G$  number of samples from  $|\psi_{\text{out}}\rangle$  in the computational basis, which means that we will have  $G$  number of rotated point sets. If we show each sample of the rotation angle with  $\theta_l$ , then the rotated points in point set are  $\mathbf{x}^i = \mathcal{T}_{\theta_l} \mathbf{m}^i$  and the points in the empirical point set are  $\mathbf{y}^j = \mathbf{s}^j$ . We calculate the expectation value of the  $\tilde{\mathcal{L}}_{\text{MMD}}$  for the samples of  $\theta_l$  to obtain a final explicit form for the MMD loss  $\tilde{\mathcal{L}}_{\text{MMD}}^f$  in terms of rotation angle

samples as

$$\tilde{\mathcal{L}}_{\text{MMD}}^f = -\frac{2}{MNG} \sum_{i,j}^{N,M} \sum_l^G \mathcal{KC}(\mathcal{T}_{\theta_l} \mathbf{m}^i, \mathbf{s}^j) \quad (28)$$

Now we use the method proposed by (Liu & Wang, 2018b) to calculate the gradients of the cost function in (28). In this approach, the quantum gates of the circuit are of the form  $U(\eta) = \exp(-i\frac{\zeta}{2}\Sigma)$ , where  $\zeta$  is the training parameter and  $\Sigma$  can be a series of unitary operators satisfying  $\Sigma^2 = I$ . As shown in (Mitarai et al., 2018), the gradient of an observable of the circuit,  $B$ , w.r.t its parameters  $\zeta$  is given by:

$$\frac{\partial \langle B \rangle_\zeta}{\partial \zeta} = \frac{1}{2} (\langle B \rangle_{\zeta^+} - \langle B \rangle_{\zeta^-}) \quad (29)$$

where  $\zeta^\pm$  are two new circuits with shifted sets of parameters from the original circuit parameters. With the mapping explained in the section 4.1, we can write the output probability distribution of the circuit as the distribution of the rotation angle,  $\theta$ , and we call it  $p_\eta(\theta)$ , where  $\eta$  is the set of training parameters for the corresponding circuits. If the observable is measured in the computational basis, we can write the gradient of the output probability,  $p_\eta(\theta)$ , as

$$\frac{\partial p_\eta(\theta)}{\partial \eta_k} = p_{\eta_k}^-(\theta) - p_{\eta_k}^+(\theta) \quad (30)$$

where the  $-1/2$  factor difference from (29) is because of a different parameterisation that is chosen in (Coyle et al., 2020). The  $\pm$  notation means that the  $k$ -th parameter in the original circuit has been shifted by  $\pm \frac{\pi}{2}$ , i.e.,  $p_{\eta_k}^\pm = p_{\eta_k \pm \pi/2}$ .

Therefore we can write the gradients of the loss (26) as:

$$\begin{aligned} \frac{\partial \mathcal{L}_{\text{MMD}}}{\partial \eta_k} &= \frac{2\mathbb{E}}{\substack{\mathbf{a} \sim \mathcal{M}^- \\ \mathbf{x} \sim \mathcal{M}}} (\mathcal{KC}(\mathbf{a}, \mathbf{x})) - \frac{2\mathbb{E}}{\substack{\mathbf{b} \sim \mathcal{M}^+ \\ \mathbf{x} \sim \mathcal{M}}} (\mathcal{KC}(\mathbf{b}, \mathbf{x})) \\ &\quad - \frac{2\mathbb{E}}{\substack{\mathbf{a} \sim \mathcal{M}^- \\ \mathbf{y} \sim \mathcal{S}}} (\mathcal{KC}(\mathbf{a}, \mathbf{y})) + \frac{2\mathbb{E}}{\substack{\mathbf{b} \sim \mathcal{M}^+ \\ \mathbf{y} \sim \mathcal{S}}} (\mathcal{KC}(\mathbf{b}, \mathbf{y})) \end{aligned} \quad (31)$$

which can be estimated as

$$\begin{aligned} \frac{\partial \tilde{\mathcal{L}}_{\text{MMD}}}{\partial \eta_k} &= \frac{2}{PNG} \sum_{p,l}^{P,G} \sum_i^N \mathcal{KC}(\mathcal{T}_{\theta_p^-} \mathbf{m}^i, \mathcal{T}_{\theta_l} \mathbf{m}^i) \\ &\quad - \frac{2}{QNG} \sum_{q,l}^{Q,G} \sum_i^N \mathcal{KC}(\mathcal{T}_{\theta_q^+} \mathbf{m}^i, \mathcal{T}_{\theta_l} \mathbf{m}^i) \\ &\quad - \frac{2}{PMN} \sum_p^P \sum_{i,j}^{N,M} \mathcal{KC}(\mathcal{T}_{\theta_p^-} \mathbf{m}^i, \mathbf{s}^j) \\ &\quad + \frac{2}{QMN} \sum_q^Q \sum_{i,j}^{N,M} \mathcal{KC}(\mathcal{T}_{\theta_q^+} \mathbf{m}^i, \mathbf{s}^j) \end{aligned} \quad (32)$$

where we have  $P, Q$  samples,  $\hat{\theta}^- = \{\theta_1^-, \dots, \theta_P^-\}$ ,  $\hat{\theta}^+ = \{\theta_1^+, \dots, \theta_Q^+\}$  drawn from the parameter shifted circuits,

$p_{\eta_k}^-(\theta), p_{\eta_k}^+(\theta)$  respectively, from which we calculate the rotated point sets  $\mathbf{a} = \mathcal{T}_{\theta_p^-} \mathbf{m}$ ,  $\mathbf{b} = \mathcal{T}_{\theta_q^+} \mathbf{m}$  and  $G$  samples,  $\hat{\theta} = \{\theta_1, \dots, \theta_G\}$  drawn from the the original Born circuit, from which we calculate the rotated point set  $\mathbf{x} = \mathcal{T}_{\theta_l} \mathbf{m}$ . The parameter shifted circuits are of the form (33):

$$|0\rangle^{\otimes n} \xrightarrow{H^{\otimes n}} \boxed{U_{l:k+1}} \xrightarrow{U_k(\eta_k^\pm)} \boxed{U_{k-1:1}} \xrightarrow{\theta^p / \theta^q \in \{0, 1\}^n} \boxed{\text{Measure}} = \quad (33)$$

where we have the definition  $U_{l:m} := U_l U_{l-1} \dots U_{m+1} U_m$ , and the  $k^{\text{th}}$  gate carries one of the Ising parameters,  $\alpha_k$  or a set of the measurement unitary parameters,  $\{\Gamma_k, \Delta_k, \Sigma_k\}$ .

## 5. Experiments

### 5.1. IQP and QAOA circuit structures

IQP and QAOA as sub-classes of the QCIBM universal class can be obtained by the following particular choice of circuit parameters (Coyle et al., 2020):

$$\begin{aligned} \text{IQP}(\{J_{ij}, b_k\}) &= \text{IBM} \left( \{J_{ij}, b_k\}, \right. \\ \left. \Gamma = \left\{ \frac{\pi}{2\sqrt{2}} \right\}, \mathbf{0}, \Sigma = \left\{ \frac{\pi}{2\sqrt{2}} \right\} \right) \end{aligned} \quad (34)$$

$$\begin{aligned} \text{QAOA}_{p=1}(\{J_{ij}, b_k\}, \Gamma) &= \text{IBM}(\{J_{ij}, b_k\}, \Gamma = -\Gamma, \mathbf{0}, \mathbf{0}) \end{aligned} \quad (35)$$

Therefore, the measurement unitary gate for the IQP simplifies to:

$$\begin{aligned} U_f^{\text{IQP}} &= U_f \left( \forall k : \Gamma_k = \frac{\pi}{2\sqrt{2}}, \Delta_k = \frac{\pi}{2\sqrt{2}}, \Sigma_k = 0 \right) \\ &= \bigotimes_{k=1}^n \exp \left( \frac{i\pi}{2\sqrt{2}} (X_k + Z_k) \right) \end{aligned} \quad (36)$$

This results in a final Hadamard gate (up to a phase factor) applied to every qubit, since:

$$H = \frac{1}{\sqrt{2}} (X + Z) \quad (37)$$

However, in a general QAOA circuit, the goal is to build the state

$$|\psi_{\hat{\gamma}, \hat{\beta}}\rangle = \prod_{i=1}^p e^{-i\beta_i \mathcal{H}_x} e^{-i\gamma_i \mathcal{H}_z} |+\rangle^{\otimes n} \quad (38)$$

where

$$\mathcal{H}_x = \sum_{i=1}^n X_i \quad (39)$$

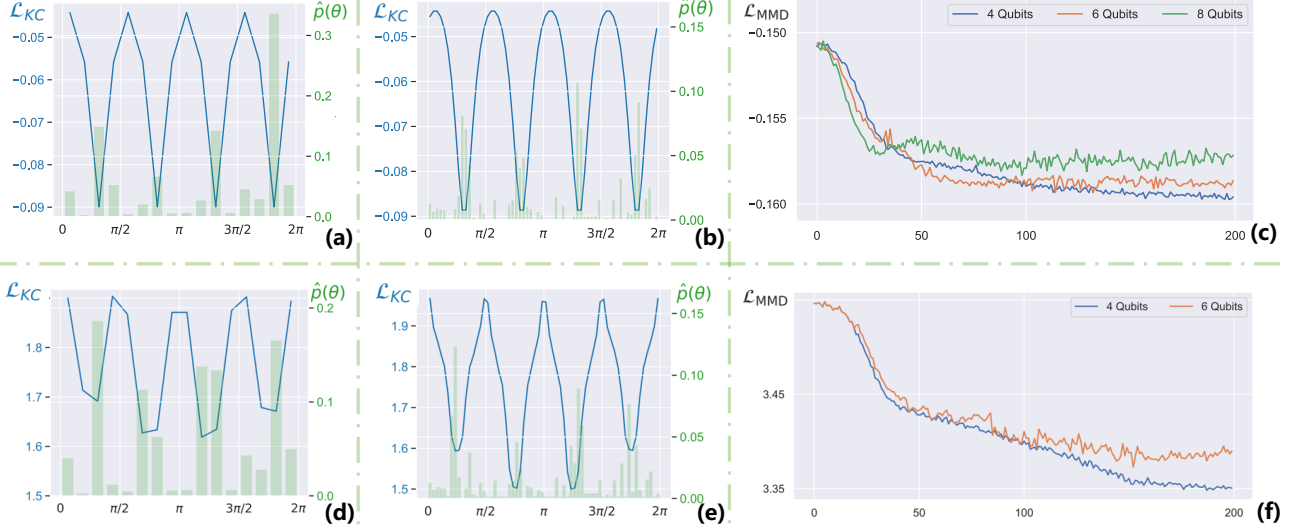


Figure 3. Proof of concept results for a 2D square shape in  $x - y$  plane, rotated by  $5\pi/16$  radian around the  $\hat{z}$ -axis: (a) and (b) show the classical KC loss function (in blue) and output angle distribution (in green) from the trained QCIBM with 4 and 6 qubits in the quantum register, respectively. The QCIBM uses  $\mathcal{L}_{\text{MMD}}$  incorporating the classical KC as the kernel function. (c) training curves of QCIBM for four, six and eight qubits (for the classical KC as kernel function). (d), (e) and (f) are the same as the first row, except that these are calculated with the quantum kernel.

and

$$\mathcal{H}_z = \sum_j \alpha_j \bigotimes_{i \in S_j} Z_i \quad (40)$$

where, one needs to optimise over the set of angles  $\{\hat{\gamma}, \hat{\beta}\} = \{\gamma_1, \dots, \gamma_p, \beta_1, \dots, \beta_p\}$  to obtain the state containing the solution to the problem. For  $p = 1$ , we have

$$|\psi_{\gamma, \beta}\rangle = e^{-i\beta\mathcal{H}_x} e^{-i\gamma\mathcal{H}_z} |+\rangle^{\otimes n} \quad (41)$$

Using (14) and (35), we can obtain the form of the measurement unitary for QAOA circuit as:

$$\begin{aligned} U_f^{\text{QAOA}} &= U_f(\forall k : \Gamma_k = -\Gamma_k, \Delta_k = 0, \Sigma_k = 0) \\ &= \exp\left(-i \sum_{k=1}^n \Gamma_k X_k\right) \end{aligned} \quad (42)$$

## 5.2. Synthesised data and training parameters

For experiments, 2D symmetric polygons inscribed by a unit circle at origin were synthesized as scene point sets and then they are rotated for a fixed angle to obtain the corresponding model point sets. Each side of these polygons consists of 10 points and the number of sides ranges from three to six.

For the training, the  $U_f$  gate parameters were set to the particular choice of parameters for IQP or QAOA circuits as explained in section 5.1, but the Ising parameters,  $\{J_{ij}, b_k\}$ , were initialised randomly. During the training, we use

Adam (Kingma & Ba, 2017) as the optimiser and the learning rate is set to  $1e-4$  initially, and is decayed by 0.5 every 50 epochs.

## 6. Results and Discussion

In this work, for the first time, a generic QCL framework is applied to the point set matching problem and the solution of the problem as a distribution of rotation angles is obtained. This framework can show quantum learning supremacy upon efficient implementation on a quantum computer. Furthermore, the loss function of the QCL model benefits from the machinery of kernel-embedding techniques to reduce the dimensionality of the problem as well as efficient assessment of the point set matching by defining a quantum kernel in RKHS.

Due to initial better performances of IQP circuit and also the time and computational resource constraints, all of the experimental results are for the IQP circuit. However, more robust performance assessments between these two circuit structures needs to be done.

As illustrated in figure 1, the symmetry of the shapes dictates multiple correct solutions to the point set matching task. Since we sample the whole possible rotation angle range to find the correct solutions, we expect to obtain a distribution with a number of peaks at the correct rotation angle and its integer multiples, residing in the range  $[0, 2\pi)$ . figure 3 shows that this expectation has been fulfilled and the

quantum approach has been successful in finding the correct distribution of angles. Furthermore, the performance of the proposed quantum approach has been bench-marked against the conventional kernel correlation approach explained in section 3 (see figure 3).

## Acknowledgements

MN would like to thank QuBiT-Lab at UCLA, ECE department for hospitality during the first stages of this work.

## References

Arute, F., Arya, K., Babbush, R., Bacon, D., Bardin, J. C., Barends, R., Biswas, R., Boixo, S., Brandao, F. G., Buell, D. A., et al. Quantum supremacy using a programmable superconducting processor. *Nature*, 574(7779):505–510, 2019.

Belkin, M., Ma, S., and Mandal, S. To understand deep learning we need to understand kernel learning. In Dy, J. G. and Krause, A. (eds.), *Proceedings of the 35th International Conference on Machine Learning, ICML*, volume 80 of *Proceedings of Machine Learning Research*, pp. 540–548. PMLR, 2018.

Besl, P. J. and McKay, N. D. A method for registration of 3-d shapes. *IEEE Transactions on Pattern Analysis and Machine Intelligence*, 14(2):239–256, 1992. doi: 10.1109/34.121791.

Biamonte, J., Wittek, P., Pancotti, N., Rebentrost, P., Wiebe, N., and Lloyd, S. Quantum machine learning. *Nature*, 549(7671):195–202, 2017.

Borgwardt, K. M., Gretton, A., Rasch, M. J., Kriegel, H.-P., Schölkopf, B., and Smola, A. J. Integrating structured biological data by kernel maximum mean discrepancy. *Bioinformatics*, 22(14):e49–e57, 2006.

Bremner, M. J., Montanaro, A., and Shepherd, D. J. Achieving quantum supremacy with sparse and noisy commuting quantum computations. *Quantum*, 1:8, 2017.

Brown, L. G. A survey of image registration techniques. *ACM computing surveys (CSUR)*, 24(4):325–376, 1992.

Chen, Y. and Medioni, G. Object modeling by registration of multiple range images. In *Proceedings. 1991 IEEE International Conference on Robotics and Automation*, pp. 2724–2729 vol.3, 1991. doi: 10.1109/ROBOT.1991.132043.

Cheng, S., Chen, J., and Wang, L. Information perspective to probabilistic modelling: Boltzmann machines versus born machines. *Entropy*, 20(8), 2018.

Cho, Y. and Saul, L. K. Kernel methods for deep learning. In Bengio, Y., Schuurmans, D., Lafferty, J. D., Williams, C. K. I., and Culotta, A. (eds.), *Advances in Neural Information Processing Systems*, pp. 342–350, 2009.

Coyle, B., Mills, D., Danos, V., and Kashefi, E. The born supremacy: quantum advantage and training of an ising born machine. *npj Quantum Information*, 6(1), Jul 2020. ISSN 2056-6387. doi: 10.1038/s41534-020-00288-9. URL <http://dx.doi.org/10.1038/s41534-020-00288-9>.

Farhi, E. and Harrow, A. W. Quantum supremacy through the quantum approximate optimization algorithm. *arXiv preprint arXiv:1602.07674*, 2016.

Farhi, E. and Neven, H. Classification with quantum neural networks on near term processors. *arXiv preprint arXiv:1802.06002*, 2018.

Farhi, E., Goldstone, J., and Gutmann, S. A quantum approximate optimization algorithm. *arXiv preprint arXiv:1411.4028*, 2014.

Geiger, A., Lenz, P., and Urtasun, R. Are we ready for autonomous driving? the kitti vision benchmark suite. In *IEEE Conference on Computer Vision and Pattern Recognition (CVPR)*, 2012.

Golyanik, V. and Theobalt, C. A quantum computational approach to correspondence problems on point sets. In *IEEE/CVF Conference on Computer Vision and Pattern Recognition (CVPR)*, 2020.

Granger, S. and Pennec, X. Multi-scale em-icp: A fast and robust approach for surface registration. In *European Conference on Computer Vision (ECCV)*, 2002.

Gretton, A., Borgwardt, K. M., Rasch, M. J., Schölkopf, B., and Smola, A. A kernel two-sample test. *The Journal of Machine Learning Research*, 13(1):723–773, 2012.

Havlíček, V., Córcoles, A. D., Temme, K., Harrow, A. W., Kandala, A., Chow, J. M., and Gambetta, J. M. Supervised learning with quantum-enhanced feature spaces. *Nature*, 567(7747):209–212, 2019.

Hofmann, T., Schölkopf, B., and Smola, A. J. Kernel methods in machine learning. *The annals of statistics*, pp. 1171–1220, 2008.

Kingma, D. P. and Ba, J. Adam: A method for stochastic optimization, 2017.

Liu, J.-G. and Wang, L. Differentiable learning of quantum circuit born machines. *Physical Review A*, 98, 2018a.

Liu, J.-G. and Wang, L. Differentiable learning of quantum circuit born machines. *Physical Review A*, 98(6):062324, 2018b.

Mitarai, K., Negoro, M., Kitagawa, M., and Fujii, K. Quantum circuit learning. *Physical Review A*, 98, 2018.

Muandet, K., Fukumizu, K., Sriperumbudur, B. K., and Schölkopf, B. Kernel mean embedding of distributions: A review and beyond. *Foundations and Trends in Machine Learning*, 10(1-2):1–141, 2017. URL <https://arxiv.org/abs/1605.09522>.

Noormandipour, M. Implementation of a quantum perceptron in intel-qs. 2020. doi: 10.5281/zenodo.3731158. URL <https://doi.org/10.5281/zenodo.3731158>.

Noormandipour, M., Sun, Y., and Haghigat, B. Restricted boltzmann machine representation for the groundstate and excited states of kitaev honeycomb model. *cond-mat.dis-nn*, [arXiv:2003.07280](https://arxiv.org/abs/2003.07280), 2021.

Preskill, J. Quantum computing in the nisq era and beyond. *Quantum*, 2:79, 2018.

Rangarajan, A., Chui, H., and Bookstein, F. L. The softassign procrustes matching algorithm. In *Biennial International Conference on Information Processing in Medical Imaging (IPMI)*, pp. 29–42, 1997.

Schuld, M. Quantum machine learning models are kernel methods. *arXiv preprint arXiv:2101.11020*, 2021.

Schuld, M. and Killoran, N. Quantum machine learning in feature hilbert spaces. *Physical review letters*, 122(4): 040504, 2019.

Shepherd, D. and Bremner, M. J. Temporally unstructured quantum computation. *Proceedings of the Royal Society A: Mathematical, Physical and Engineering Sciences*, 465(2105):1413–1439, 2009.

Sriperumbudur, B. K., Fukumizu, K., Gretton, A., Schölkopf, B., and Lanckriet, G. R. On integral probability metrics, phi-divergences and binary classification. *arXiv preprint arXiv:0901.2698*, 2009.

Torlai, G., Mazzola, G., Carrasquilla, J., Troyer, M., Melko, R., and Carleo, G. Neural-network quantum state tomography. *Nature Physics*, 14(5), Feb 2018.

Tsin, Y. and Kanade, T. A correlation-based approach to robust point set registration. In *European conference on computer vision (ECCV)*, 2004.

Wittek, P. (ed.). *Quantum Machine Learning*. Boston, 2014.

Zeng, A., Song, S., Nießner, M., Fisher, M., Xiao, J., and Funkhouser, T. 3dmatch: Learning local geometric descriptors from rgb-d reconstructions. In *IEEE Conference on Computer Vision and Pattern Recognition*, 2017.

Zhang, Z. Iterative point matching for registration of free-form curves and surfaces. *International journal of computer vision*, 13:119–152, October 1994.

Zhong, H.-S., Wang, H., Deng, Y.-H., Chen, M.-C., Peng, L.-C., Luo, Y.-H., Qin, J., Wu, D., Ding, X., Hu, Y., Hu, P., Yang, X.-Y., Zhang, W.-J., Li, H., Li, Y., Jiang, X., Gan, L., Yang, G., You, L., Wang, Z., Li, L., Liu, N.-L., Lu, C.-Y., and Pan, J.-W. Quantum computational advantage using photons. *Science*, 2020.

Zhu, H., Guo, B., Zou, K., Li, Y., Yuen, K.-V., Mihaylova, L., and Leung, H. A review of point set registration: From pairwise registration to groupwise registration. *Sensors*, 19(5), 2019. ISSN 1424-8220. doi: 10.3390/s19051191. URL <https://www.mdpi.com/1424-8220/19/5/1191>.

## Appendix

### A. A QUBOP Approach on an Adiabatic Quantum Annealer

In a work by (Golyanik & Theobalt, 2020) the point set matching is formulated as finding the optimal  $n$  dimensional bit string ( $\mathbf{q} \in \mathbb{B}^n$ ) that minimises the quadratic energy term:

$$\mathbf{q}^{opt} = \arg \min_{\mathbf{q} \in \mathbb{B}^n} \mathbf{q}^\top \Phi \Phi^\top \mathbf{q} \quad (43)$$

where  $\Phi$  is defined based on some iterated correspondence of  $\mathcal{M}$  and  $\mathcal{S}$ , and a basis of rotation matrices ( $\{\mathbf{Q}_k\}_{k=1}^K$ )<sup>2</sup>:

$$\Phi = - \begin{pmatrix} -\mathbf{m}_1^\top & -\mathbf{m}_2^\top & \dots & -\mathbf{m}_N^\top \\ (\mathbf{Q}_1 \mathbf{s}_1)^\top & (\mathbf{Q}_1 \mathbf{s}_2)^\top & \dots & (\mathbf{Q}_1 \mathbf{s}_N)^\top \\ (\mathbf{Q}_2 \mathbf{s}_1)^\top & (\mathbf{Q}_2 \mathbf{s}_2)^\top & \dots & (\mathbf{Q}_2 \mathbf{s}_N)^\top \\ \vdots & \vdots & & \vdots \\ (\mathbf{Q}_K \mathbf{s}_1)^\top & (\mathbf{Q}_K \mathbf{s}_2)^\top & \dots & (\mathbf{Q}_K \mathbf{s}_N)^\top \end{pmatrix} \quad (44)$$

$$\Phi \Phi^\top = - \begin{pmatrix} -\sum_i \mathbf{m}_i^\top \mathbf{m}_i & \dots & \sum_i \mathbf{m}_i^\top \mathbf{Q}_K \mathbf{s}_i \\ \sum_i \mathbf{s}_i^\top \mathbf{Q}_1 \mathbf{m}_i & \dots & \sum_i \mathbf{s}_i^\top \mathbf{Q}_1^\top \mathbf{Q}_K \mathbf{m}_i \\ \sum_i \mathbf{s}_i^\top \mathbf{Q}_2 \mathbf{m}_i & \dots & \sum_i \mathbf{s}_i^\top \mathbf{Q}_2^\top \mathbf{Q}_K \mathbf{m}_i \\ \vdots & & \vdots \\ \sum_i \mathbf{s}_i^\top \mathbf{Q}_K \mathbf{m}_i & \dots & -\sum_i \mathbf{s}_i^\top \mathbf{Q}_K^\top \mathbf{Q}_K \mathbf{m}_i \end{pmatrix} \quad (45)$$

here we note  $L_{\mathcal{MS}}(\mathbf{m}_i) = \mathbf{s}_i$  just for simplicity. Clearly, (45) is a real symmetric matrix since  $\sum_i \mathbf{x}_i^\top \mathbf{Q}_K \mathbf{y}_i =$

<sup>2</sup>for the detailed design of  $\{\mathbf{Q}_k\}$  for 2D and 3D point sets, please refer to section 5.1 and 5.2 of (Golyanik & Theobalt, 2020)

$\sum_i \mathbf{y}_i^\top \mathbf{Q}_K \mathbf{x}_i$ , hence the objective in (43) becomes:

$$\mathbf{q}^{opt} = \arg \min_{\mathbf{q} \in \mathbb{B}^n} \sum_i \sum_{j>i} (\Phi \Phi^\top)_{ij} \quad (46)$$

subject to  $q_i = q_j = 1$

A more general case is to have multiple correspondence:

$$\Phi = [\Phi_1; \Phi_2; \dots; \Phi_N] \quad (47)$$

where  $\Phi_i$  represents all the corresponding points of  $\mathbf{m}_i$ :

$$\Phi_i = - \begin{pmatrix} -\mathbf{m}_i^\top & -\mathbf{m}_i^\top & \dots & -\mathbf{m}_i^\top \\ (\mathbf{Q}_1 \mathbf{s}_{L_1}^i)^\top & (\mathbf{Q}_1 \mathbf{s}_{L_2}^i)^\top & \dots & (\mathbf{Q}_1 \mathbf{s}_{L_n}^i)^\top \\ (\mathbf{Q}_2 \mathbf{s}_{L_1}^i)^\top & (\mathbf{Q}_2 \mathbf{s}_{L_2}^i)^\top & \dots & (\mathbf{Q}_2 \mathbf{s}_{L_n}^i)^\top \\ \vdots & \vdots & & \vdots \\ (\mathbf{Q}_K \mathbf{s}_{L_1}^i)^\top & (\mathbf{Q}_K \mathbf{s}_{L_2}^i)^\top & \dots & (\mathbf{Q}_K \mathbf{s}_{L_n}^i)^\top \end{pmatrix} \quad (48)$$

here  $\mathbf{s}_L^i = \{\mathbf{s}_{L_1}^i, \mathbf{s}_{L_2}^i, \dots, \mathbf{s}_{L_n}^i\} = L_{\mathcal{MS}}(\mathbf{m}_i)$ , that is, each point in  $\mathcal{M}$  has  $n$  correspondents in the other set  $\mathcal{S}$ . Similar with multi-linked ICP, (Golyanik & Theobalt, 2020) solve  $L_{\mathcal{MS}}(\mathbf{m}_i)$  with alternating nearest neighbour assignments which also suffers from the local minimum traps. Instead, kernel correlation essentially is a fully linked affinity that probes for the global minima.